ENCIT 2018

ABCM Associação Brasileira de Engenharia e Ciências Mecânicas

17th Brazilian Congress of Thermal Sciences and Engineering
November 25th-28th, 2018, Águas de Lindóia, SP, Brazil

ENCIT-2018-0039
ANALYSIS OF MAGNETIC FLUID DISPLACEMENT IN CAPILLARIES

Douglas Daniel de Carvalho
Rafael Gabler Gontijo
Universidade Estadual de Campinas, Faculdade de Engenharia Mecânica, Departamento de Energia, Campinas, SP-Brazil, 13083-860
douglascarvalho47@gmail.com
rafaelgabler@gmail.com

Francisco Ricardo da Cunha
Universidade de Brasília, Departamento de Engenharia Mecânica, Campus Darcy Ribeiro, Brasília, DF-Brazil, 70910-900
frcunha2@gmail.com

Abstract. *This work consists of a theoretical, numerical and experimental study to determine both the shape and vertical displacement of a free surface formed between a ferrofluid and a non-magnetic fluid, confined between two vertical plates. The presence of an external magnetic field applied by a permanent magnet arbitrarily positioned in space is considered. A new mathematical model is proposed, leading to a nonlinear differential equation that governs both the shape and the vertical displacement of the free surface due to capillary and magnetic effects. The applied field considered in this work satisfies the Ampère-Maxwell equation in the magnetostatic limit. This equation is numerically solved by direct integration using a fourth order Runge-Kutta method, coupled with a Newton-Raphson scheme. The numerical code is validated by means of some analytical solutions valid on specific asymptotic limits and by experimental results. Experimental measurements of surface tension, density and vertical displacement of Newtonian fluids in capillaries are also presented. Contact angles were also calculated. The influence of the variation of the physical variables concerning the physics of the problem on the shape and on the vertical displacement is evaluated. An increase in the intensity of the magnetic effects resulted in an increase in the vertical displacement and in the asymmetric degree of the free surfaces.*

Keywords: *magnetic fluids, capillarity, magnetic pressure, meniscus shape/displacement, contact angle calculations*

1. INTRODUCTION

Ferrofluids are stable colloidal suspensions of magnetic particles that magnetize strongly in the presence of an external magnetic field. They combine the hydrodynamic properties of ordinary fluids with the opportunity to interact with magnetic fields, which gives rise to various applications (John *et al.*, 2011), both technological and biomedical (Cunha, 2012; Scherer and Neto, 2005), for example the displacement of magnetic fluids in porous media due to capillary and magnetic effects. In one study, (Rosensweig *et al.*, 2005) measured the displacement and the shape of a ferrofluid meniscus in response to an uniform magnetic field, finding that the meniscus displacement in a flat vertical wall decreases to horizontally applied fields, increases in vertically applied fields, and does not change in fields applied parallel to the wall. In another publication, the authors concluded that the magnetic field changes the pressure jump on the meniscus (Bashtovoi *et al.*, 2005). Some studies of the ferrofluid meniscus shape along vertical cylindrical wires that carry electric current evidenciated that the viscosity of the magnetic fluid has no influence on the final shape of the meniscus around the wire, however changes in the contact angle may influence the meniscus on the entire container (Eissmann *et al.*, 2011; John *et al.*, 2011). In a recent paper, (Gontijo *et al.*, 2016) investigated the behavior of the shape as well as the vertical displacement of a ferrofluid meniscus in the presence of a vertical magnetic field. Among other conclusions, the authors showed that even for conditions where the interface has a small curvature, it would be possible to make a displacement of the fluid interface with a combination of low capillary pressure being compensated by moderate magnetic pressure effects.

2. PROBLEM UNDER STUDY

This work aims to determine both the shape and the vertical displacement of a bidimensional free surface formed on the interface between a ferrofluid and a non-magnetic fluid between two parallel vertical flat plates. The fluids are considered to be under the influence of an external magnetic field applied by a permanent magnet arbitrarily positioned in space. Figure 1 shows the sketch of the problem considered.

The ferrofluid is taken to be fluid 1 and the non-magnetic fluid, fluid 2. The space between the two plates is $2c$. The

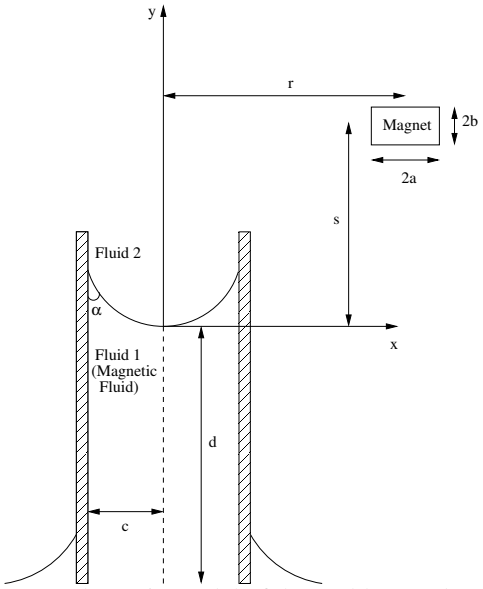

Figure 1: Schematic model of the problem under study

height *d* denotes the vertical displacement of the free surface. The permanent magnet is arbitrarily positioned at *s* and *r*, and has dimensions *2a* and *2b*. The contact angle formed between fluid 1 and the parallel walls is given by α.

2.1 General governing equations

This work proposes a new mathematical model for the study of the mentioned bidimensional free surface. The physics of the problem is governed by the combined action of capillary, magnetostatic and gravitational forces along with the contact angle (Boudouvis *et al.*, 1988). The extensive algebraic manipulations performed will not be presented here, as they are similar to those presented by (Gontijo *et al.*, 2016). The main physical principles and their representation in mathematical symbolic notation are presented below.

Young-Laplace pressure jump:

$$\Delta p = 2\gamma \bar{K} \tag{1}$$

Where $\Delta p = (p_1\text{-}p_2)$ is the pressure jump on the interface, p_1 is the pressure on fluid 1, p_2 is the pressure on fluid 2, γ is the surface tension and $\bar{K}$ is the interface mean curvature, given by Eq. (2):

$$\bar{K} = \frac{y''}{2(1+y'^2)^{\frac{3}{2}}} \tag{2}$$

Here, *y' = dy/dx* is the first derivative of shape funcion *y* and *y" =* d^2y/dx^2 is the second derivative.

Maxwell equations in the magnetostatic limit:

$$\nabla \times \boldsymbol{H} = \mathbf{0} \tag{3}$$

$$\nabla \cdot \boldsymbol{B} = 0 \tag{4}$$

Where $\boldsymbol{B}$ represents the magnetic induction vector, $\boldsymbol{H}$ represents the magnetic field vector and ∇ denotes the vectorial nabla operator. In the present context, the ferrofluid under analysis is taken as a superparamagnetic fluid, in this case:

$$\boldsymbol{M} = \chi \boldsymbol{H} \tag{5}$$

χ is the magnetic susceptibility and $\boldsymbol{M}$ represents the magnetization, a measurement of the degree of alignment of the particles dipole moments within the fluid in the direction of the applied field. If all magnetic moments are aligned with the the direction of the applied field, the magnetization is called saturation magnetization: $\boldsymbol{M_s}$ (Cunha, 2012).

Vector quantities $\boldsymbol{B}$, $\boldsymbol{H}$ and $\boldsymbol{M}$ are related by:

$$\boldsymbol{B} = \mu_0(\boldsymbol{H} + \boldsymbol{M}) \tag{6}$$

Here, $\mu_0 = 4\pi \times 10^{-7} H/m$ is the magnetic permeability of free space.
Hydrostatic fundamental equation:

$$-\nabla \cdot \boldsymbol{\sigma} = \rho \boldsymbol{g} \tag{7}$$

ρ is the fluid density, $\boldsymbol{\sigma}$ is the fluid stress tensor and $\boldsymbol{g}$ is the gravitational field. The stress tensor of a continuous magnetic fluid is represented by the sum of the effects of the carrier fluid and the magnetic particles, resulting in a hydrodynamic and magnetic contribution (Cunha, 2012). This way:

$$\boldsymbol{\sigma}(\boldsymbol{x}, t) = -\Big[p(\boldsymbol{x}, t) + p_m(\boldsymbol{x}, t)\Big]\boldsymbol{I} + \boldsymbol{BH} \tag{8}$$

Where p is the static pressure, $\boldsymbol{I}$ is the Kronecker Delta tensor, p_m is the magnetic pressure given by Eq. (9):

$$p_m = \frac{\mu_0}{2}(\boldsymbol{H} \cdot \boldsymbol{H}) \tag{9}$$

Thus, after algebraic manipulations, the hydrostatic fundamental equation for a magnetic fluid is obtained:

$$\nabla p = \mu_0 \boldsymbol{M} \cdot \nabla \boldsymbol{H} + \rho \boldsymbol{g} \tag{10}$$

It is noticed the presence of a magnetic contribution term, which is called Kelvin's force density (Rosensweig, 1985):

$$\boldsymbol{f}_m = \mu_0 \boldsymbol{M} \cdot \nabla \boldsymbol{H} \tag{11}$$

Magnetic boundary conditions, as presented in (Rosensweig, 1985), where the subscripts *"t"* and *"n"* represent the tangential and normal projections, respectively, according to Fig. 2:

$$B_{1n} = B_{2n} \quad \text{and} \quad H_{2t} = H_{1t} \tag{12}$$

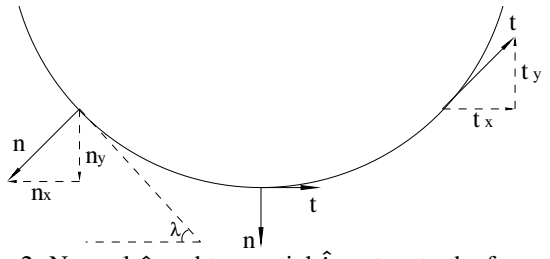

Figure 2: Normal $\hat{\boldsymbol{n}}$ and tangential $\hat{\boldsymbol{t}}$ vectors to the free surface

Table 1: Components analysis

	$Y'(X) \geq 0$	$Y'(X) < 0$
n_x	$\lvert \sin[\arctan(Y'(X))] \rvert$	-$\lvert \sin[\arctan(Y'(X))] \rvert$
n_y	-$\lvert \cos[\arctan(Y'(X))] \rvert$	-$\lvert \cos[\arctan(Y'(X))] \rvert$
t_x	$\lvert \cos[\arctan(Y'(X))] \rvert$	$\lvert \cos[\arctan(Y'(X))] \rvert$
t_y	$\lvert \sin[\arctan(Y'(X))] \rvert$	-$\lvert \sin[\arctan(Y'(X))] \rvert$

Normal components of $\boldsymbol{B}$ and tangential components of $\boldsymbol{H}$ are continuous through the interface (Gontijo *et al.*, 2016).
The stress jump on the interface between the two fluids is given, for an homogeneous membrane, by (Cunha, 2012):

$$\Delta \boldsymbol{f}_i = \boldsymbol{n} \cdot ||\sigma_1 - \sigma_2|| = 2\gamma \bar{K} \hat{\mathbf{n}} \tag{13}$$

σ_i is the stress tensor, $\Delta \boldsymbol{f}_i$ is the interfacial force and depends on the characteristis of the fluids (Cunha, 2012).
Thus, after extensive algebraic manipulations, we arrive at an equation for y". The quantities on this equation were then made non-dimensional through the following relations:

$$Y = \frac{y}{c} \qquad X = \frac{x}{c} \qquad D = \frac{d}{c} \qquad \tilde{H}_{2n} = \frac{H_{2n}}{M_s} \qquad \tilde{H}_{2t} = \frac{H_{2t}}{M_s} \tag{14}$$

The non-dimensional equation obtained for *Y"* is given by Eq. (15):

$$Y'' = \left(1+Y'^2\right)^{\frac{3}{2}}\left\{\left(\frac{\Delta\rho gc}{\gamma/c}\right)(D+Y)+\left(\frac{\mu_0 M_s^2}{2\gamma/c}\right)\tilde{H}_{2n}^2\left[\frac{(1+\chi_2)^2}{(1+\chi_1)}-(1+\chi_2)\right]+\left(\frac{\mu_0 M_s^2}{2\gamma/c}\right)\tilde{H}_{2t}^2(\chi_2-\chi_1)\right\} \tag{15}$$

In Equation (15), $\tilde{H}_{2t}$ and $\tilde{H}_{2n}$ are the tangential and normal components of vector $\boldsymbol{H}$ on fluid 2:

$$\tilde{H}_{2t}^2 = G(X,Y,Y',\tilde{H}_{0y},\tilde{H}_{0x}) = (t_x t_x \tilde{H}_{0x} + t_y t_x \tilde{H}_{0y})^2 + (t_x t_y \tilde{H}_{0x} + t_y t_y \tilde{H}_{0y})^2 \tag{16}$$

$$\tilde{H}_{2n}^2 = F(X,Y,Y',\tilde{H}_{0y},\tilde{H}_{0x}) = (n_x n_x \tilde{H}_{0x} + n_y n_x \tilde{H}_{0y})^2 + (n_x n_y \tilde{H}_{0x} + n_y n_y \tilde{H}_{0y})^2 \tag{17}$$

Where H_{0x} and H_{0y} are the components of the applied magnetic field and, n_x, n_y, t_x, t_y are the components of the normal and tangential vectors to the interface:

$$n_x = t_y = \sin(\lambda) \quad \text{and} \quad n_y = t_x = \cos(\lambda) \tag{18}$$

λ is the arc-tangent of the first derivative of the function *Y(X)*: $\lambda = \arctan[Y'(X)]$.

This work considers the exact solution for an external and irrotational magnetic field applied by a rectangular permanent magnet with uniform polarity, where the components in the *x* and *y* directions are presented in (McCaig and Clegg, 1987), where $J = \mu_0 M_i$ and M_i is taken to be the internal magnet magnetization. Making the quantities non-dimensional, it leads to: $\tilde{H}_{0y} = H_{0y}/M_s$; $\tilde{H}_{0x} = H_{0x}/M_s$; *A=a/c*; *B=b/c*; *R = r/c* and *S = s/c*.

$$H_{0x} = \frac{J}{4\pi\mu_0} ln\left\{\frac{y+b+\left[(y+b)^2+(x-a)^2\right]^{\frac{1}{2}}}{y-b+\left[(y-b)^2+(x-a)^2\right]^{\frac{1}{2}}} \times \frac{y-b+\left[(y-b)^2+(x+a)^2\right]^{\frac{1}{2}}}{-y+b+\left[(-y+b)^2+(x+a)^2\right]^{\frac{1}{2}}}\right\} \tag{19}$$

$$H_{0y} = \frac{J}{4\pi\mu_0} ln\left\{\frac{x+a+\left[(y-b)^2+(x+a)^2\right]^{\frac{1}{2}}}{x-a+\left[(y-b)^2+(x-a)^2\right]^{\frac{1}{2}}} \times \frac{x-a+\left[(y+b)^2+(x-a)^2\right]^{\frac{1}{2}}}{x+a+\left[(y+b)^2+(x+a)^2\right]^{\frac{1}{2}}}\right\} \tag{20}$$

We notice in Eq. (15) two important dimensionless parameters, the Bond number and its magnetic version, given by:

$$Bo = \frac{\Delta\rho gc}{\gamma/c} \tag{21}$$

$$Bo_m = \frac{\mu_0 M_s^2}{2\gamma/c} \tag{22}$$

Finally, the final dimensionless equation is obtained, which governs the shape and the displacement of the free surface.

$$Y'' = \left(1+Y'^2\right)^{\frac{3}{2}}\left\{Bo(D+Y)+Bo_m\left\{F(X,Y,Y',\tilde{H}_{0y},\tilde{H}_{0x})\left[\frac{(1+\chi_2)^2}{(1+\chi_1)}-(1+\chi_2)\right]+G(X,Y,Y',\tilde{H}_{0y},\tilde{H}_{0x})(\chi_2-\chi_1)\right\}\right\} \tag{23}$$

The associated physical variables are: the magnetic susceptibilities of the fluids under analysis χ_1 and χ_2, the Bond and magnetic Bond numbers, components H_{0x} and H_{0y} of the external applied magnetic field, which are functions of the permanent magnet dimensions (*2A* and *2B*), its spatial position (*R* and *S*), as well of the parameter $M_i/4\pi M_s$, which represents the dimensionless magnet intensity. Boundary conditions for Eq. (23) are given below:

$$Y'(1) = cot(\alpha) \quad \text{and} \quad Y'(-1) = -cot(\alpha) \tag{24}$$

The geometric restriction *Y(0) = 0* indicates the origin of the coordinate system.

2.2 Governing equations for the experimental section

Balance of forces acting on a Newtonian non-magnetic fluid drop contained in a capillary (Cengel and Cimbala, 2015):

$$W - F_b = F_\gamma \rightarrow \rho_1 g(\pi R^2 d) - \rho_2 g(\pi R^2 d) = 2\pi b\gamma cos(\alpha) \tag{25}$$

W is the volume weight, F_b is the buoyancy force, $F_\gamma = 2b\pi\gamma cos(\alpha)$ is the vertical component of the force generated by the surface tension. Here, *R* is the radius of the free surface. This way, the contact angle α is given by:

$$\alpha = arccos\left(\frac{\Delta\rho g b d}{2\gamma}\right) \tag{26}$$

2.3 Analytical solutions

For all analytical solutions presented here, the assumption that $Y'^2 \ll 1$ was imposed, so that the mean curvature of the meniscus was reduced, through a non-dimensional Eq. (2), to $\bar{K} = Y''/2$.

By eliminating the magnetic contribution terms in Eq. (23), we obtain an equation which governs the asymptotic limit where both fluids are considered non-magnetic:

$$Y'' = \left(1 + Y'^2\right)^{\frac{3}{2}}\Big[Bo(D + Y)\Big] \tag{27}$$

Analytical solutions for vertical displacement and free surface format for Eq. (27) are presented in (Gontijo *et al.*, 2016), and are shown in Tab. 2. Table 2 also presents an equation for vertical displacement for the magnetic case.

Table 2: Analytical solutions. Solutions 2.1, 2.2, 2.3 and 2.4 are presented in (Gontijo *et al.*, 2016).

Non-magnetic Case			
Constant Curvature		Variable Curvature	
Shape (2.1)	$Y(X) = X[cot(\alpha) - cos(\alpha)] + X^2\frac{cos(\alpha)}{2}$	Shape (2.2)	$Y(X) = -D + \frac{cot(\alpha)\, cosh(\sqrt{Bo}X)\, csch(\sqrt{Bo})}{\sqrt{Bo}}$
Vertical Displacement (2.3)	$D_c = \frac{cos(\alpha)}{Bo}$	Vertical Displacement (2.4)	$D_0 = \sqrt{Bo}D_c\left[\frac{csch(\sqrt{Bo})}{sin(\alpha)}\right]$
Constraints of Application	$Bo \ll 1 + sen(\alpha)$ e $cot(\alpha) \ll 1$	Constraints of Application	$cot(\alpha) \ll 1$
Magnetic Case			
Constant Curvature			
Vertical Displacement (2.5)	$D_m = D_c - \frac{Bo_m}{Bo}\left\{\tilde{H}_{0x}^2(\chi_2 - \chi_1) + \tilde{H}_{0y}^2\left[\frac{(1+\chi_2)^2}{(1+\chi_1)} - (1+\chi_2)\right]\right\}$		
Constraints of Application	$cot(\alpha) \ll 1$		

3. METHODOLOGY

3.1 Numerical

Equation (23) was numerically integrated by means of a numerical code developed in *FORTRAN* by the authors. This code computes both the vertical displacement *D* and the shape $Y = \mathcal{F}(X, Bo, Bo_m, \alpha, \chi_1, \chi_2, \tilde{H}_{0y}, \tilde{H}_{0x})$ of the free surface. The problem is transformed into an initial value problem, using an iterative scheme coupled to the Newton-Rhapson method, in order to accelerate the convergence of the numerical solution. Equation (23) was numerically integrated using a fourth-order Runge-Kutta scheme, using the boundary conditions given in Eq. (24) and the geometrical restriction. A fully description of a similar algorithm used in the numerical code is found in (Gontijo *et al.*, 2016).

3.2 Experimental

An experimental set (Fig. 3-(a)) was built in order to determine the vertical displacement of Newtonian fluids in capillary tubes with different internal diameters. The density and surface tension of these fluids were also measured using the facilities of the Laboratory of Michohydrodynamics and Rheology of the Vortex group of the Universidade de Brasília. Contact angles for each of the analyzed fluids in each of the capillary tubes were calculated, using Eq. (26).

3.2.1 Materials

- Fluids: Distilled water, glycerin and mineral oil.
- 5 capillary tubes with different diameters: $1000 \pm 50\mu$m, $500 \pm 20\mu$m, $300 \pm 10\mu$m, $150 \pm 5\mu$m and $100 \pm 5\mu$m.
- Densimeter *Anto Paar DMA 38*.
- Tensiometer *LAUDA TVT 2*.

3.2.2 Procedures

The capillary tubes were allocated in the experimental set and the fluids placed inside the reservoir. The process of vertical displacement by capillary effects then began. After a certain time, where no noticeable change in vertical displacement was observed, the displaced fluid columns were photographed next to a ruler.

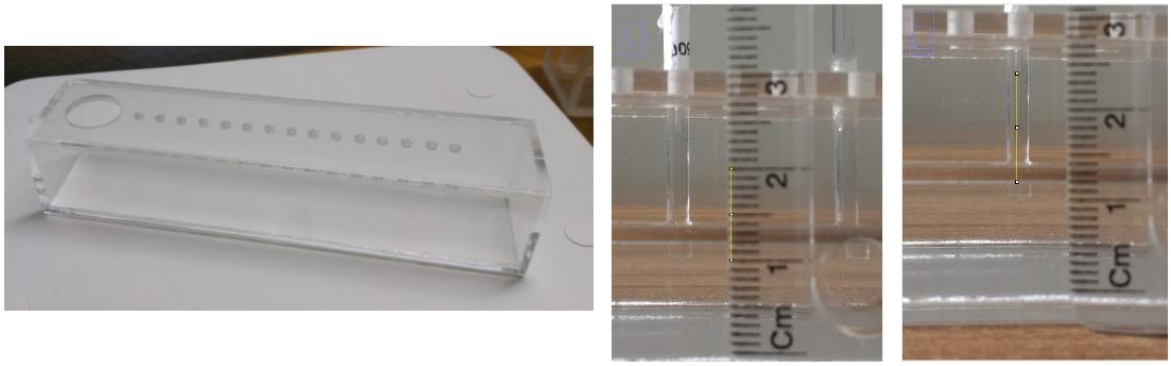

(a) (b) (c)

Figure 3: (a) Experimental set; (b) Selection of the base length. (c) Selection of vertical displacement. Tube with $500 \pm 20\mu$m of internal diameter, distilled water

The images were then analyzed by means of a software (*ImageJ*) that operates according to a measurement comparison system, one measurement predetermined by the user (Fig. 3-(b)), and another arbitrarily selected in the image (Fig. 3-(c)). 12 measurements were performed for each fluid in each capillary. The largest and the smallest of these measures were discarded and the means and standard deviations of the remaining 10 measurements were taken. The uncertainty of each measurement is given by the sum of the standard deviation and half the resolution of the ruler, here being 0.5mm.

Densities and surface tensions of the fluids were measured using the oscillating U tube type densimeter *Anto Paar DMA 38* and the tensiometer *LAUDA TVT 2*, which operates according to the pending drop method, respectively.

4. RESULTS AND DISCUSSIONS

4.1 Numerical code validation

In this section, a test of the numerical integration scheme of Eq. (23) was performed, and the results obtained were compared with the analytical solutions presented in Tab. 2, in order to validate them.

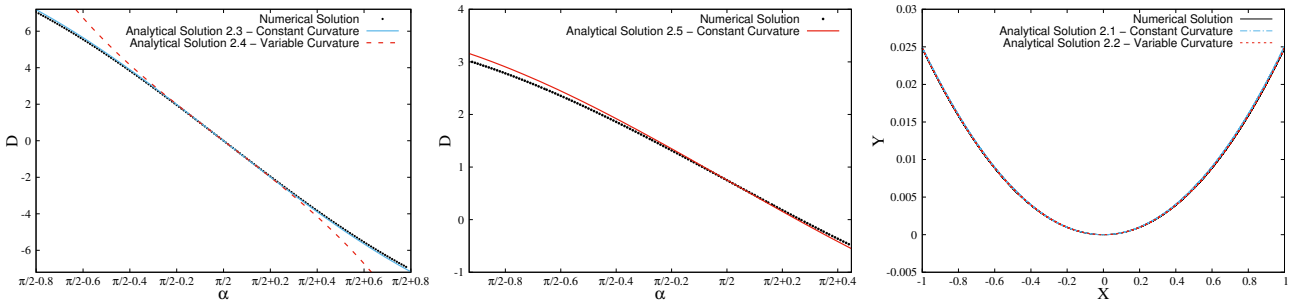

(a) (b) (c)

Figure 4: (a) and (b) Vertical displacement as a function of the variation of the contact angle; (c) Free surface shapes. For (a): Non-magnetic case and Bo = 1/10. For (b): Magnetic case and Bo = 1/3; Bo_m = 1/2; $\chi_1 = 1.0$; $\chi_2 = 3.6 \times 10^{-7}$; 2A = 2B = 5.0; R = -13.0; S = 12.0 and $M_i/4\pi M_s$ = 10.0. For (c): Non magnetic case and Bo = 1/10 and $\alpha = \pi/2 - 0.05$.

From Figures 4-(a) and (b) it is possible to see a remarkable agreement between the numerical and analytical results around $\alpha = \pi/2$, for both the non-magnetic and magnetic cases, respectively. The results diverge for angles not close enough to $\alpha = \pi/2$, as in those cases the constraint of application ($cot(\alpha) << 1$) is not properly met. Figure 4-(c) shows an excellent agreement between the shapes obtained for the free surfaces format. Thus, the numerical results are validated. The developed numerical code will be used to study cases where the analytical solutions may not be suitably used. A further validation will be presented when the numerical results are compared to the experimental ones.

4.2 Results obtained for the non-magnetic case

4.2.1 Numerical results

Vertical displacement

Figure 5-(a) shows that the vertical displacement "*D*" decreases as the Bond number increases. A 10 times increase in *Bo* caused a decrease of approximately 11 times in *D*. *Bo* (Eq. (21)) is a measurement of the relative magnitude between hydrostatic and capillary pressures (Gontijo *et al.*, 2016), capillary forces being responsible both for the fluid rise and to overcome the gravitational action produced by the hydrostatic ones. An increase in *Bo* is achieved by an increase in hydrostatic pressures, which inhibits the capillary rise, justifying the obtained decrease in *D*. In practice, this increase is achieved by an enlargement of the distance between the parallel plates "*2c*", which leads to conditions where the capillary effects are insignificant or even negligible.

From Figure 5-(b) it is seen that for $\alpha < \pi/2$ there is fluid rise (*D* > 0), yet for $\alpha > \pi/2$ there is fluid involution (*D* < 0). As $|\alpha - \pi/2|$ increases, both for $\alpha < \pi/2$ and $\alpha > \pi/2$ scenarios, higher fluid displacements are observed. It happens due to the presence of more intense curvature effects, which can be either positive or negative, and consequently, bigger capillary pressure effects are observed, resulting in higher fluid displacements, both positive and negative. For symmetric contact angles (i.e. $\pi/2 \pm 0.05$), the vertical displacements obtained were also symmetrical, (i.e. D = $\pm$0.491, respectively). For $\alpha = \pi/2$, *D* = 0, as in this condition $\bar{K}$ = 0, and therefore there is no pressure jump at the interface.

Free surface shapes

Figures 6-(a) and (b) present numerical results for the free surface shapes as a function of the contact angle α. Variations on α produce different menisci shapes. All shapes obtained are symmetrical with respect to the *Y* axis. In order to consider a vertical symmetry, it must be stated, according to (Gontijo *et al.*, 2016), that *Y'(0) = 0*, meaning the derivatives must be null at the origin, which is valid in these cases, as shown by the detail in Figure 6-(a). Figure 6-(a) shows concave menisci, yet Fig. 6-(b) shows convex ones. This happens due to the wettability property, which is a result from intermolecular interactions that occur when the fluid and the solid wall are held in contact, whose degree is determined by a balance between adhesion and cohesion forces. Figures 6-(a) and (b) show that systems with contact angles $\alpha < \pi/2$ produce concave menisci - adhesion forces > cohesion forces -, while systems with contact angles $\alpha > \pi/2$ produce convex menisci - cohesion forces > adhesion forces -. In the magnetic case, due to the presence of asymmetric magnetic forces related to the magnet placement in space, null derivatives in the origin are not considered.

4.2.2 Experimental results

Vertical displacements, contact angles, densities and surface tensions

Vertical displacements, surface tensions and densities were measured according to the procedures shown in section 3.2.2. The experimental conditions were numerically simulated, and a comparison among the obtained results is presented in Tab. 3, as well as contact angles, densities and surface tensions. Measurements taken at 25^{o}C.

Table 3: Displacements, surface tensions and densities. D_{num} = numerical and D_{exp} = experimental displacements.

	Distilled Water			Glycerin			Mineral Oil		
	ρ = 997 $\pm$ 1 Kg/m^3		γ = 0.07088 $\pm$ 0.00010 N/m	ρ = 1258 $\pm$ 1 Kg/m^3		γ = 0.06272 $\pm$ 0.00024 N/m	ρ = 866 $\pm$ 1 Kg/m^3		γ = 0.02648 $\pm$ 0.00044 N/m
Internal Diameter [μm]	D_{exp}	D_{num}	Contact Angle [°]	D_{exp}	D_{num}	Contact Angle [°]	D_{exp}	D_{num}	Contact Angle [°]
1000 $\pm$ 50	6.99 $\pm$ 1.30	6.95	83.1 $\pm$ 1.3	5.34 $\pm$ 1.32	5.30	82.5 $\pm$ 1.8	16.39 $\pm$ 2.04	16.16	49.1 $\pm$ 4.7
500 $\pm$ 20	47.89 $\pm$ 4.39	47.83	78.1 $\pm$ 1.1	28.16 $\pm$ 3.19	28.10	80.1 $\pm$ 0.9	78.09 $\pm$ 6.65	77.80	38.7 $\pm$ 2.2
300 $\pm$ 10	141.90 $\pm$ 10.15	141.83	77.3 $\pm$ 0.9	130.08 $\pm$ 9.49	129.99	73.3 $\pm$ 0.6	170.17 $\pm$ 12.00	169.95	52.3 $\pm$ 1,1
150 $\pm$ 5	783.98 $\pm$ 53.05	783.89	72.3 $\pm$ 1.2	544.74 $\pm$ 37.23	544.65	72.5 $\pm$ 0.3	1022.94 $\pm$ 68.78	1022.59	23.1 $\pm$ 0.8
100 $\pm$ 5	1665.88 $\pm$ 167.07	1665.81	73.4 $\pm$ 1.6	1364.26 $\pm$ 137.08	1364.17	70.5 $\pm$ 0.3	-	-	-

Table 3 shows that for distilled water, glycerin and mineral oil, the maximum differences between D_{exp} and D_{num} were about 0.57%, 0.81% and 1.41%, respectively. The numerical results were also able to validate the numerical code.

4.3 Numerical results for the magnetic case

4.3.1 Vertical displacement

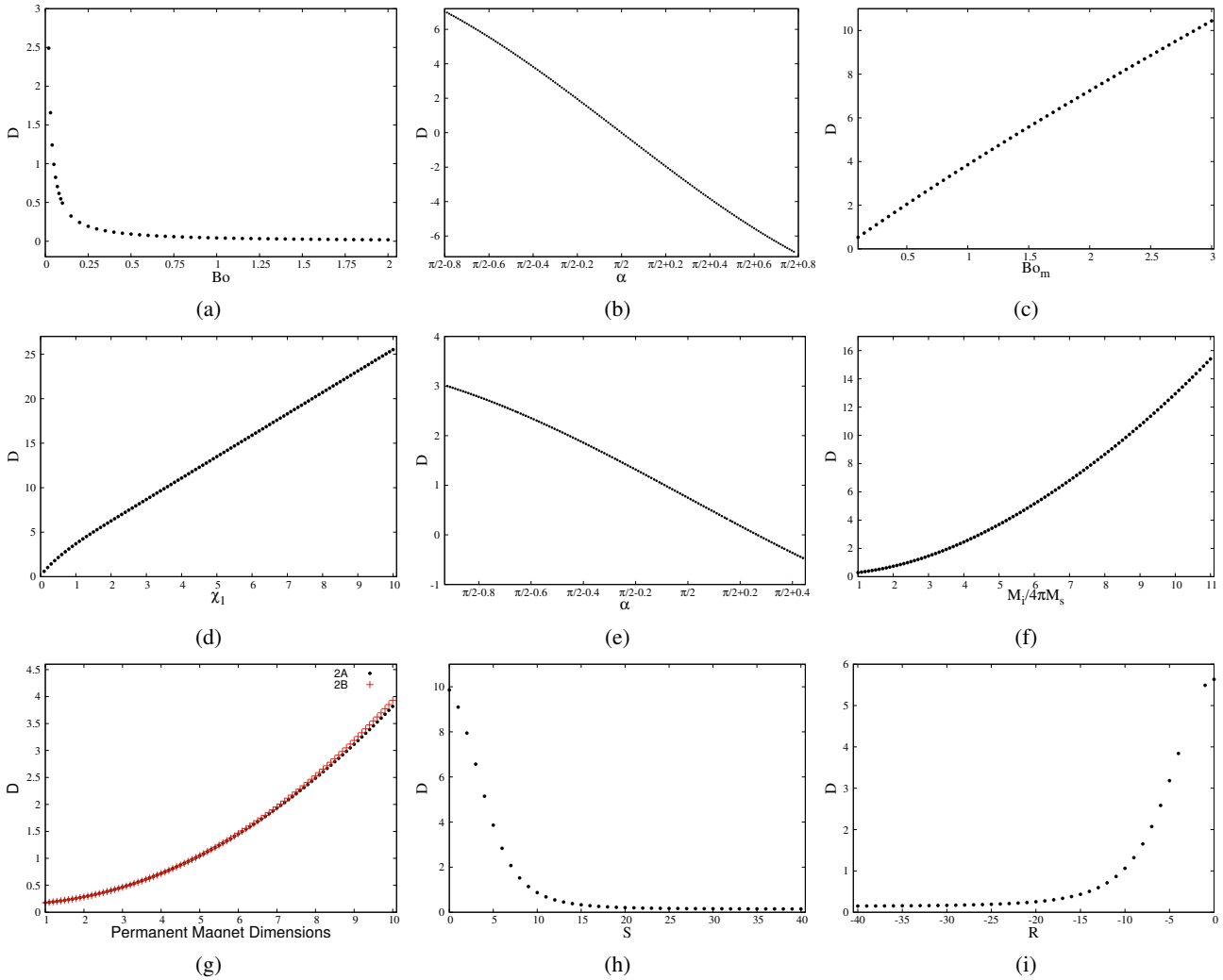

Figure 5: Vertical displacements as a function of the variation of: (a) Bond number - Non magnetic case; (b) Contact angle - Non magnetic case; (c) Magnetic Bond number; (d) Ferrofluid's magnetic susceptibility (e) Contact angle - Magnetic case; (f) Dimensionless intensity of the magnet; (g) Magnet dimensions; (h) Magnet vertical position; (i) Magnet horizontal position. For (a): $\alpha = \pi/2 - 0.05$. For (b): Bo = 1/10. For (c): Bo = 1/3; $\alpha = \pi/2 - 0.05$; χ_1=1; χ_2=3.6 $\times 10^{-7}$; 2A = 2B = 6; R = -9; S = 8 and $M_i/4\pi M_s$ = 5. For (d): Bo = 1/3; Bo_m = 1/2; $\alpha = \pi/2 - 0.05$; χ_2=3.6 $\times 10^{-7}$; 2A = 2B = 7; R = -9; S = 8 and $M_i/4\pi M_s$ = 5. For (e): Bo = 1/3; Bo_m = 1/2; χ_1=1; χ_2=3.6 $\times 10^{-7}$; 2A = 2B = 5; R = -13; S = 12 and $M_i/4\pi M_s$ = 10. For (f): Bo = 1/3; Bo_m = 1/2; $\alpha = \pi/2 - 0.05$; χ_2=3.6 $\times 10^{-7}$; 2A = 2B = 7; R = -9; S = 8. For (g): Bo = 1/3; $\alpha = \pi/2 - 0.05$; χ_1=1; χ_2=3.6 $\times 10^{-7}$; R = -9; S = 8; $M_i/4\pi M_s$ = 5; For the black dots: 2B = 5; For the red cross: 2A = 5. For (h): Bo = 1/3; $\alpha = \pi/2 - 0.05$; χ_1=1; χ_2=3.6 $\times 10^{-7}$; 2A = 2B = 5; R = -7 and $M_i/4\pi M_s$ = 5. For (i): Bo = 1/3; $\alpha = \pi/2 - 0.05$; χ_1=1; χ_2=3.6 $\times 10^{-7}$; 2A = 2B = 5; S = 7 and $M_i/4\pi M_s$ = 5.

Figure 5-(c) shows that the vertical displacement *D* increases with Bo_m. A 10 times increase in Bo_m caused an increase of approximately 7 times in *D*. Bo_m (Eq. (22)) is a measurement of the relative magnitude between the magnetic and capillary pressures (Gontijo *et al.*, 2016). An increase in Bo_m is achieved by an increase in magnetic pressures, which act in order to increase the pressure jump at the interface, and thereby causing a higher vertical displacement, even under adverse conditions of fluid rising, where capillary effects may be negligible (i.e capillaries with big diameters).

Figure 5-(d) shows that *D* increases with the ferrofluid magnetic susceptibility χ_1. A 10 times increase in χ_1 resulted in an increase of approximately 7 times in *D*. Considering χ as a percentage measurement of the number of particles lining up to the magnetic field and that the fluid under analysis in superparamagnetic (Eq. (5)), it is assumed that the particles magnetic dipole moments align in the direction of the field as soon as it is applied (instantaneous response time). As the value of χ_1 is increased, the state of magnetic polarization of the medium is increased, in other words, it increases the

extent to which the fluid is magnetized. An increase in the magnetization of the fluid causes an increase in Kelvin's force density (Eq. (11)), resulting in a bigger interface pressure jump, leading to an increase in *D*.

Figure 5-(e) shows that as the contact angle α increases, *D* decreases until there is no more fluid rise, yet fluid involution. Under the analyzed physical conditions, this behavior occurred at $\alpha = \pi/2 + 0.265$. It is noticed that even at $\alpha \geq \pi/2$, it is possible to move fluid vertically upward due to the presence of magnetic effects (associated with magnetic pressures), as opposed to the observed in the non-magnetic case. For conditions where the free surface has a small curvature, it is also possible to carry out a vertical upward displacement, due to a combination of low capillary pressures being compensated by magnetic effects. In this case, the pressure jump is not null at the interface in the presence of an external magnetic field. The idea behind that would be to promote a displacement in capillaries with not necessarily too small internal diameters (i.e. porous media with high permeabilities).

Figures 5-(f), (g), (h) and (i) show that an increase in dimensions, in dimensionless intensity and in the proximity of the permanent magnet to the interface causes *D* to increase. A 10 times increase in $M_i/4\pi M_s$ resulted in an approximately 22 times bigger *D*; a 10 times increase in *2B* resulted in an approximately 52 times greater *D* and an increase of 10 times in *S* resulted in a decrease in *D* of roughly 10 times. Increases in $M_i/4\pi M_s$, *2A* and *2B* will generate bigger magnetic effects at the interface, since magnetic fields of higher magnitudes will be generated by magnets with bigger dimensions and intensities. As $\nabla \boldsymbol{H}$ is proportional to Kelvin's force density (Eq. (11)), its increase will result in a greater force, consequently producing a higher *D*. In addition, according to the manufacturer of magnets "*Supermagnete*", analyzing two magnets with different sizes and magnetization classification among its products, the larger the magnet, the stronger it will be, even though its magnetization classification is smaller (Supermagnete, n.d.). As for the proximity of the permanent magnet to the interface, the closer it is to the interface the higher the intensity of $\boldsymbol{H}$ will be, as given by (Cunha, 2012), $\boldsymbol{H} = \frac{\mathscr{P}\hat{\boldsymbol{r}}}{4\pi\mu_0 r^2}$, where $\boldsymbol{r}$ is an arbitrarily position in space, $\hat{\boldsymbol{r}}$ is an unit vector on the direction of $\boldsymbol{r}$ and $\mathscr{P}$ is an intensity of magnetic poles. $\boldsymbol{H}$ has a $1/r^2$ decay, so as r decreases (increasing the proximity of the permanent magnet to the free surface), the intensity of $\boldsymbol{H}$ increases. After a specific position, there is no longer a significant vertical displacement, indicating that $\boldsymbol{H}$ has decayed to an intensity unable to cause a significant pressure jump at the interface.

4.3.2 Free surface shapes

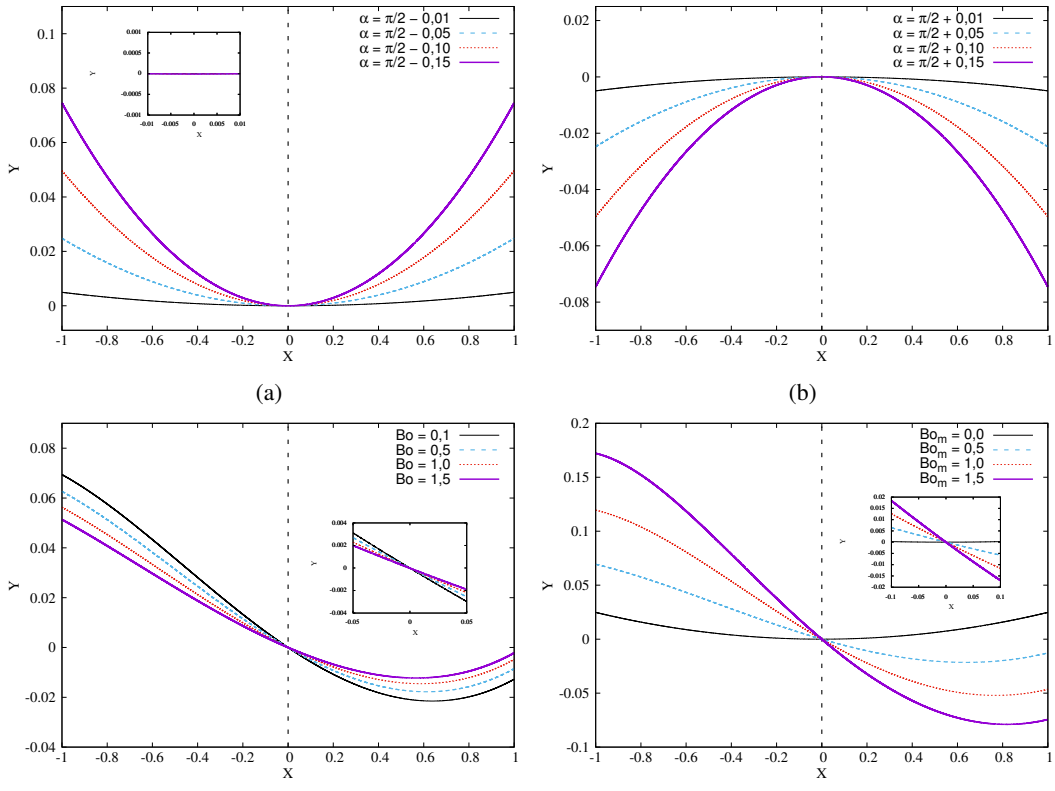

Figure 6: Free surface shapes. (a), (b) Non magnetic case; (c), (d) Magnetic case. For (a), (b) and (d): Bo = 1/10. For (c) and (d): $\chi_1 = 1$; $\chi_2 = 3.6 \times 10^{-7}$; $\alpha = \pi/2 - 0.05$; 2A = 2B = 6; R = -9; S = 8 and $M_i/4\pi M_s$ = 5. For (c): Bo_m = 1/2.

Figure 6-(c) shows that *Bo* variations result in different free surface shapes. An increase in the asymmetry of the curves is obtained as *Bo* decreases. Decreasing *Bo* leads to a decrease in hydrostatic effects (Eq. (21)), causing the capillary and

magnetic effects to become more proeminent. These results seem to suggest that an increase in the deviation of the symmetry condition is a measurement of the intensity of the magnetic effects (Gontijo *et al.*, 2016). It is seen that Y(-1) > Y(1), indicating that the left side of the meniscus is subjected to more intense magnetic effects, which is true, as under the analyzed conditions the magnet lies to the left of the origin. The asymmetric degree between the left and right sides of the curve ($\Delta = Y(-1) - Y(1)$) increases as *Bo* decreases, so does the derivatives in the center, as the detail in Fig. 6-(c) indicates. This behavior of a greater elevation of the portion of the meniscus closer to the permanent magnet was observed in all analyzed cases. Thus, if the magnet is to the right of the origin of the coordinate axes, Y(1) > Y(-1).

Figure 6-(d) shows free surface formats for a fixed *Bo* and different Bo_m. An increase of Bo_m tends to render the free surfaces increasingly asymmetrical, indicating a more complex and less linear behavior not only of the meniscus shape, but of its curvature. We postulate that this may lead to more prominent pressure jumps on the interface and hence to higher vertical displacements due to a combined action of magnetic and capillary effects. Here again, in the absence of magnetic effects (curves for Bo_m = 0), the free surface obtained is symmetric. Figure 6-(d) confirms that an increase in the deviation of the symmetry condition is a measurement of the intensity of the magnetic effects. The assumption that there may be a vertical symmetry in the menisci shape would obviously lead to an unrealistic behavior of the free surfaces. As discussed in (Gontijo *et al.*, 2016), to assume a vertical symmetry we must state that *Y'(0) = 0*, which is not valid in these cases. The only derivatives we are fully sure come from the physics of the problem, which are the ones on the vertical plates, since they depend exclusively on the contact angle, which is a physical property of the fluid-wall contact interaction. The detail in Fig. 6-(d) shows that as Bo_m, the derivatives at the center also increase, not being nulls. An increasing in the asymmetric degree as the intensity of the magnetic effects is increased was obtained in the analysis of all magnetic physical variables of the problem.

5. CONCLUSIONS

In this work it was possible to verify physical conditions where a greater vertical displacement of fluid in capillaries can be obtained. Summarizing, an increase in the intensity of the magnetic effects resulted in higher vertical displacements and asymmetric degrees of the free surfaces. One of the main findings of this work is that the distortion of the shape of the free surface due to magnetic effects lead to a more prominent displacement in capillaries. This behaviour occours due to two mechanisms: 1) the direct rise of a fluid volume against the action of gravity due to Kelvin forces and 2) the distortion of the interface due to magnetic effects that locally alter the pressure jump in combination with capillary effects.

6. ACKNOWLEDGEMENTS

The authors wish to acknowledge the support of this work by FAPESP-Brazil under the grant number 2017/05643-8.

7. REFERENCES

Bashtovoi, V., Bossis, G., Kuzhir, P. and Reks, A., 2005. "Magnetic field effect on capillary rise of magnetic fluids". *J Magn Magn Mater*, , No. 289, p. 376–378.

Boudouvis, A.G., Puchalla, J.L. and Scriven, L.E., 1988. "Interaction of capillary wetting and fringing magnetic field in ferrofluid systems". *J Colloid Interface Sci*, , No. 124, p. 677–687.

Cengel, Y.A. and Cimbala, J.M., 2015. *Mecânica dos fluidos-3*. AMGH Editora.

Cunha, F.R., 2012. *Fundamentos da Hidrodinâmica de Fluidos Magnéticos, Turbulência - V. 8 (Book Chapter)*. EPTT.

Eissmann, P.B., Lange, A. and Odenbach, S., 2011. "Meniscus of a magnetic fluid in the field of a current-carrying wire: two dimensional numerical simulations". *Magnetohydrodynam-ics*, , No. 47.

Gontijo, R.G., Malvar, S., Sobral, Y.D. and Cunha, F.R., 2016. "The influence of a magnetic field on the mechanical behavior of a fluid interface". *Meccanica - An International Journal of Theoretical and Applied Mechanics*, , No. 51.

John, T., Mat, K. and Stannarius, R., 2011. "Meniscus of a ferrofluid around a vertical cylindrical wire carrying electric current". *Phys Rev E*, , No. 83.

McCaig, M. and Clegg, A.G., 1987. *Permanent Magnets in Theory and Practice*. New York. Wiley, 2nd edition.

Rosensweig, R.E., 1985. *Ferrohydrodynamics*. Press Syndicate of the University of Cambridge, New York.

Rosensweig, R.E., Elborai, S., Lee, S.H. and Zahn, M., 2005. "Theory and measurements of ferrofluid meniscus shape in applied uniform horizontal and vertical magnetic fields". *J Magn Magn Mater*, , No. 289, p. 192–195.

Scherer, C. and Neto, A.M.F., 2005. "Ferrofluids: Properties and applications". *Brazilian Journal of Physics*, , No. 3.

Supermagnete, n.d. "What do the specifications n42, n45, n50, etc. mean?" URL `https://www.supermagnete.de/eng/faq/What-do-the-specifications-N42-N45-N50-etc-mean`.

8. RESPONSIBILITY NOTICE

The authors are the only responsible for the printed material included in this paper.